Int. J. Electrochem. Sci., 12 **(2017)** 8006 – 8020, doi: 10.20964/2017.09.11

International Journal of
ELECTROCHEMICAL
SCIENCE
www.electrochemsci.org

Investigation on Electrochemical Corrosion of 304 Stainless Steel under Thin Electrolyte Layers Containing Chloride Ions

Xuequn Cheng, Hong Luo, Kui Xiao, Chaofang Dong[*],

Corrosion and Protection Center, University of Science and Technology Beijing, Beijing 100083, China
[*]E-mail: cfdong@ustb.edu.cn

Received: 31 May 2017 / *Accepted:* 29 June 2017 / *Published:* 13 August 2017

The corrosion behaviour of 304 stainless steel (304 SS) under thin electrolyte layers containing chloride ions was studied by potentiodynamic polarization and electrochemical impedance spectroscopy (EIS). Data obtained from potentiodynamic polarization tests show that a reduction in the electrolyte layer thickness result in a negative shift of the pitting potential for 304 SS. Results that were collected from EIS analysis are also consistent with the potentiodynamic polarization curves, demonstrating a decrease in R_{ct} . This decrease indicates corrosion rate increase as the layer thickness decrease. Optical morphologies also reveal an increased amount of small corrosion pits under thinner electrolyte layers.

Keywords: A. 304 stainless steel; A. thin electrolyte layer; B. Potentiodynamic polarization; B. EIS; C. pitting corrosion

1. INTRODUCTION

304 SS has been extensively used in various industrial areas such as chemical equipment, nuclear fusion equipment, and marine application, due to its excellent machinability, weld-ability, and non-magnetic property[1-3]. However, this kind of alloy is very susceptible to pitting corrosion in chloride-containing environments. In particular, marine atmospheric environments have posed a great threat to the application of 304 SS due to the deposition of high chloride containing airborne sea salts on the metal surface [4]. In previous reports, much effort has been made to investigate the relationship between pitting corrosion and surface roughness. It was found that samples with a smoother surface finish contained a higher Cr concentration in the surface film, exhibiting a smaller frequency of pitting [5-8]. Therefore, it is important that studies are conducted into the corrosion behaviours and regimes of

stainless steel in marine atmospheric conditions. This is essential to the selection and evaluation of stainless steels which are to be used under such extreme conditions.

Despite the fact that the corrosion behaviour of 304 SS was well investigated under various conditions in bulk solution, results obtained in bulk solution can not be used to assess the corrosion behaviour under atmospheric conditions. Generally, atmospheric corrosion occurs under a thin electrolyte layer, in which the corrosion processes in terms of mass transport of ions, concentration of dissolved oxygen, and the accumulation of corrosion products differ from that of corrosion in a bulk solution [9].

In 1964, Tomashov [10] presented a model and theoretically implied that the corrosion rate is promoted in decreasing electrolyte layers, until the layer reaches 1 μm. Tsutsumi [11] studied the pitting corrosion mechanism of stainless steel under droplets of $MgCl_2$ solutions, and discovered the corrosion progresses preferentially in the horizontal direction under very thin layers, unlike a deep-type pit formed in bulk chloride solutions. Regarding the limitations of conventional electrochemical techniques for study of the atmospheric corrosion, several advanced techniques for monitoring atmospheric corrosion have been developed based on the fact that atmospheric corrosion occurs on a metal surface covered with a thin dilute electrolyte layer formed through condensation or adsorption. For instance, Stratmann [11-14] introduced scanning Kelvin probe as a non-intrusive method, allowing measurements of the Volta potential distribution on the surface of the electrode, but there is no constant relationship between Volta potential and corrosion potential when electrode and solution are subjected to change during test. In addition, the oscillation of the Kelvin probe during measurement can induce a convective effect in the thin electrolyte layer on the electrode surface. Nishikata and Tsuru [15, 16] developed a two-electrode cell to study atmospheric corrosion by EIS; however, the uneven current distribution should always be considered when analysing the EIS data. Therefore, the conventional electrochemical techniques, combined with new electrolyte layer control system, have regained interest to study atmospheric corrosion.

To date, there has been limited work conducted into the corrosion behaviour of 304 SS in marine atmospheric environment. In this work the pitting corrosion behaviour of 304 SS under various electrolyte layers containing chloride ions was investigated by employment of potentiodynamic technique and EIS through a home-made device with the ability to control the thickness of electrolyte layer. Pit morphologies were then observed by optical microscopy after the electrochemical tests. Special attention has been paid to the effects of the thickness of the thin electrolyte layers, concentration of chloride ions on pitting corrosion behaviour.

2. MATERIALS AND EXPERIMENTAL METHODS

2.1 Materials and solution

All the test specimens used in this work were prepared from a sheet of 304 SS; the chemical composition of 304 SS is given in Table 1.

Table 1. Material composition (wt. %).

C	Si	Mn	P	S	Cr	Ni
0.06	0.68	1.22	0.030	0.019	18.59	8.52

The specimens were cut into 10 mm×10 mm×2 mm, and then embedded in a two-component epoxy resin leaving an exposed surface area of 1.0 cm^2. The exposed surface of the electrode was subsequently grounded with 240 grit, 600 grit, 800 grit, and 1200 grit SiC paper, degreased with ethanol and rinsed with distilled water and then dried. The test solutions were prepared from distilled water and NaCl (AR) with concentrations of 0.1 wt. %, 0.5 wt. % and 3.5 wt. %.

2.2 The determination of the electrolyte thickness

The experimental setup used to control the thickness of the electrolyte layers on the sample surface is schematically shown in Fig.1; the detailed description of this experimental arrangement has been reported by Cheng [17].

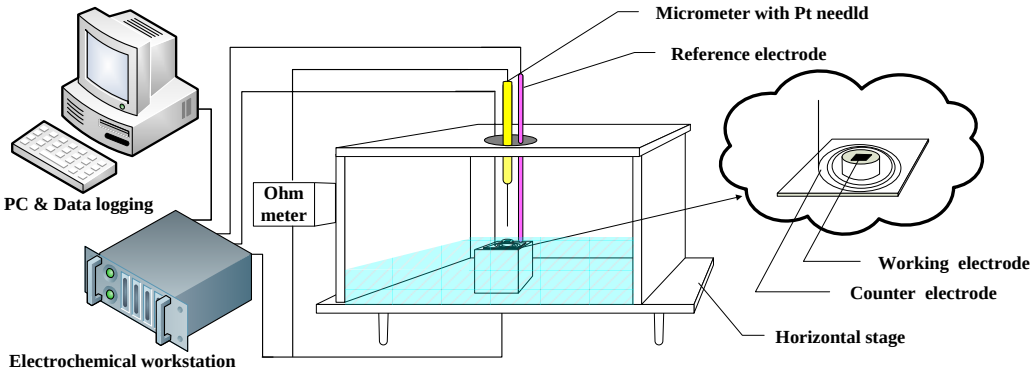

Figure 1. The schematic diagram of the device to control the electrolyte thickness on top of the sample.

The electrochemical cell was placed on an adjustable horizontal stage with a gradienter to level the sample surface; allowing the electrolyte film to be uniformly distributed on the whole electrode surface. In order to keep the thickness of electrolyte layer constant during tests, a Perspex lid was used to cover the cell and Vaseline was also applied to minimize the evaporation-induced change of electrolyte layer thickness.

The principle for determination of electrolyte layer thickness is briefly introduced as follows. A very fine platinum needle was soldered on the spindle of micrometer screw gauge, and then the micrometer screw gauge was fixed at a position right above the electrode, as shown in Fig.1. In order to form the needed electrolyte layer thickness on the electrode, a syringe was used to add or remove electrolyte through a hole in the lid. When the cell was arranged, the platinum needle was adjusted

slowly towards the electrode through micrometer screw gauge. If the tip of the platinum needle touched the electrolyte surface, the reading of ohm meter immediately decreased, with further movement of the needle, the reading of ohm meter became zero when the needle tip touched the electrode surface, then the thickness was calculated based on two readings of micrometer screw gauge with an accuracy of 1.0 μm. In addition, the three holes present in the Perspex lid for Pt-needle, counter electrode and reference electrode were sealed with Vaseline to prevent the evaporation of any electrolyte after this measurement.

2.3. Electrochemical measurements

A PARSTAT 2273 Workstation was used to perform the electrochemical measurements. A three-electrode cell equipped with counter electrode, reference electrode and the prepared specimen as working electrode were employed. A platinum multi-coils surrounded the work electrode was adopted as the counter electrode, a saturated calomel electrode (SCE) as the reference electrode which was arranged to be as close as possible to the work electrode. The advantage of this arrangement is that both the counter and reference electrode were still immersed in the bulk electrolyte, minimizing the ohmic drop between the reference electrode and the working electrode. All the electrode potentials were reported relative to SCE. Experiments were conducted at room temperature approximately 25 ^{o}C. Prior to each electrochemical test, the specimen was cathodically polarised for 5 minutes at -0.8 V_{SCE} to remove the pre-existed oxide film, then the open-circuit potential was monitored for 1 h to ensure that the system to be tested was stable. EIS was measured under a sinusoidal excitation potential of 10 mV in the frequency range from 200 kHz to 1 mHz. Fittings of the EIS plots were made by using Zview software. Potentiodynamic polarization tests were conducted at a scanning rate of 1.0 mV/s from negative to positive direction under several electrolyte layers. Optical morphologies of 304 SS after pitting corrosion were obtained with a POLYVAR MET Reichert-Jung optical microscope.

3. RESULTS AND DISCUSSION

3.1 Effects of electrolyte layer thickness on corrosion behaviour of 304 SS

Fig.2 shows the polarization curves measured for 304 SS in 0.5 wt. % NaCl under different layers.

The corresponding electrochemical parameters obtained from potentiodynamic polarization curves such as corrosion current density (i_{corr}), pitting corrosion potential (E_p), corrosion potential (E_{corr}) and Tafel slopes (β_a and β_c) are shown in Table 2.

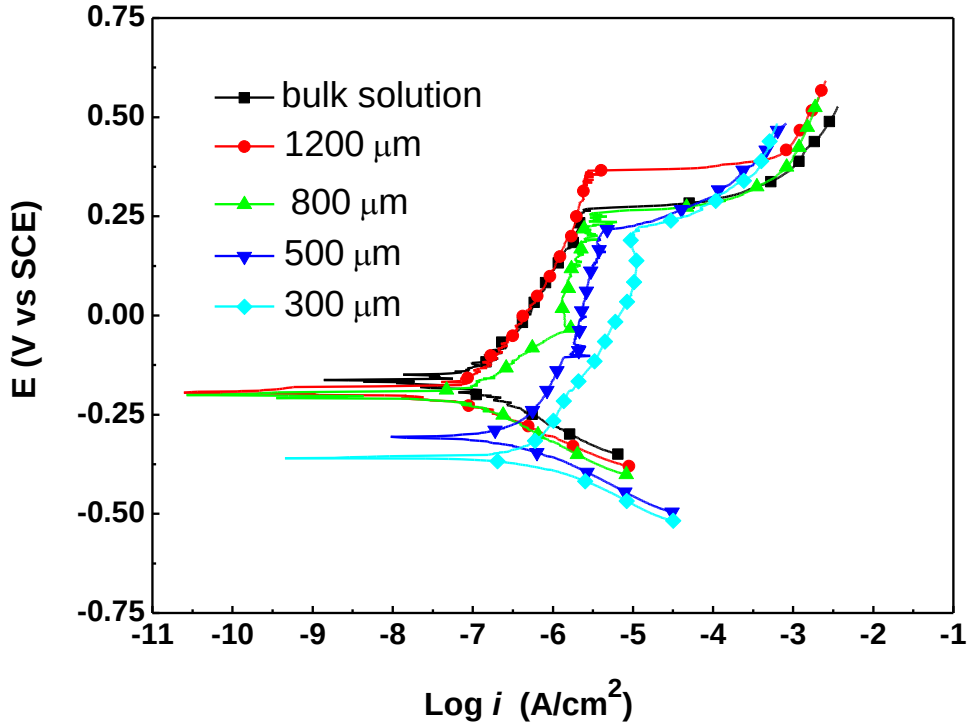

Figure 2. Polarization curves measured for 304 SS in 0.5 wt. % NaCl under different layers.

Table 2. Electrochemical parameters for 304 SS in 0.5 wt. % NaCl under different layers.

Layer thickness (μm)	E_{corr} (mV_{SCE})	i_{corr} ($\mu A\ cm^{-2}$)	β_a ($mV\ decade^{-1}$)	β_c ($mV\ decade^{-1}$)	E_p (mV_{SCE})
Bulk solution	-166	0.10	228	110	268
1200	-193	0.14	376	95	364
800	-200	0.11	143	112	263
500	-305	0.42	396	110	217
300	-358	0.71	498	99	224

The anodic Tafel region for SS is usually small due to passivity, so calculated values of i_{corr}, β_a and β_c are mainly based on the cathodic polarization region (weak anodic polarization for exceptional

cases). It was found that the i_{corr} of the samples with thin electrolyte layer demonstrated a higher corrosion current, were as the samples in the bulk solution demonstrated a decrease in i_{corr}. It can also be seen that the current density increased as the electrolyte layer thickness decreased. This may be due to the increase of the oxygen diffusion which led to the enhancement of cathodic depolarization, and well corresponding Tomashov's model: corrosion rate decreases under thin electrolyte layers from 1 μm to 1000 μm [10]. In fact, the i_{corr} of SS exists in the mere part of anodic region representing the formation of the passive film. Evans [18, 19] and Mansfeld [20, 21] proposed that it is easy for oxygen to reach the surface of the stainless steel sample during the cathodic reaction because of the thin electrolyte layer. The corrosion rates for most metals and alloys mainly depend on the depletion of oxygen and the environments in which they interact with i.e. neutral or weak acidic atmospheric environments. The β_a and β_c are the Tafel slopes for the cathodic and the anodic processes respectively. Analysing these coefficients demonstrates that as the thickness of the electrolyte layers increase, the values of the β_a/β_c decreased and E_p increased.

The potential at which the current density exceeded 10^{-2} A/cm^2 was identified as the pitting potential (E_p). The corrosion behaviour was evaluated by the absolute value of the pitting potential (E_p), the corrosion current density (i_{corr}), the passive current density (i_p) and the corrosion potential (E_{corr}). These values were all obtained from the polarization curves.

It is known that oxygen reduction is the main cathodic reaction on the electrode in a neutral solution. The kinetics of reduction reaction, and hence anodic dissolution, are strongly influenced by the transfer of charge across the metal-solution interface to dissolved oxygen and the transfer of the dissolved oxygen. For the thick electrolyte layer, the electrolyte layer consists of two parts: a diffusion layer (inner layer) and a convection layer. Because the change of the layer thickness mainly affects the convection layer, the diffusion limiting current remains constant. Due to the action of surface tension, the control of continuous layer less than 300 μm is hard to obtain technically and needs to be improved further, thus the layer thickness from 200 μm to 2000 μm had no apparent influence on the cathodic current density [17].

The values of the passive current (shown in table 2) were very small indicating a good protection efficiency of 304 SS. Once the passive film had been formed, the reaction rate between the metal and the environment would be several orders of magnitude lower. According to the authors [21], the passive film formed in the solution could have two processes: the chromium-rich passive film could dissolve into the solutions and the chromium from the matrix of stainless steel could diffuse into the metal surface forming new passive layers. As the thickness of the electrolyte layers decreased, the first process was much faster than the second process. Thus, the decrease in electrolyte layer made it easier for the film to get thinner and could lead to the film rupture. Moreover, recent investigations [23-25] discovered the correlation between oxide film weakening and the sudden onset of corrosion, which was observed and explained by an explosive autocatalytic growth in the number of metastable pits with the formation of stable, individual pits taking place later. It was also found that when i_p increased under the thin electrolyte layers, the amount of metastable pits also multiplied, again leading to the formation of stable pits. Consequently E_p decreased under thinner electrolyte layers. Fig.3 shows pit morphologies of 304 SS in 0.5 wt. % NaCl after polarization under different layers: (a) 500 μm; (b) 1200 μm.

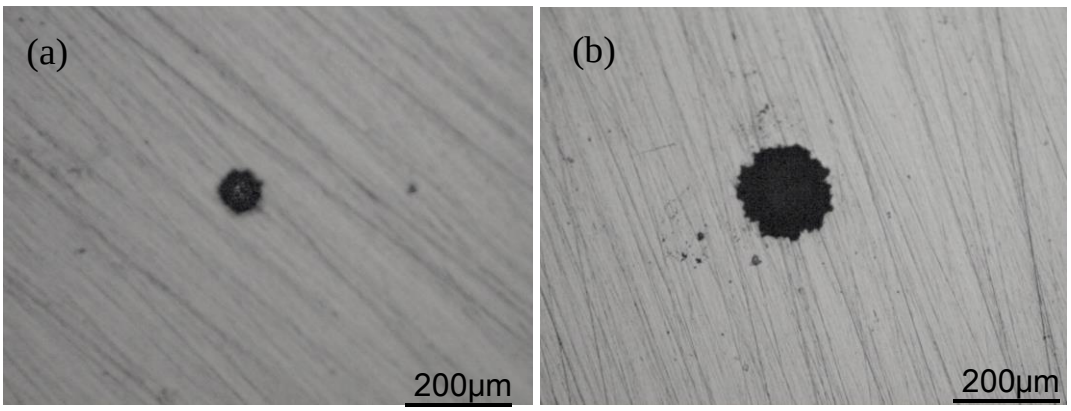

Figure 3. Pits morphologies of 304 SS in 0.5 wt. % NaCl after polarization under different layers: (a) 500 μm; (b) 1200 μm.

The pits formed under thicker electrolyte layer are apparently bigger than that formed in thinner layers. Generally it is difficult to hydrate or transport in thinner water layers for dissolved metal ions; therefore the growth of pits was restrained.

In order to further understand the atmospheric corrosion behaviour of 304 SS, EIS measurements were carried out at the open-circuit potential under the thin electrolyte layers (0.5 wt. % NaCl). Fig.4 shows the EIS results of the samples under the thin electrolyte layers.

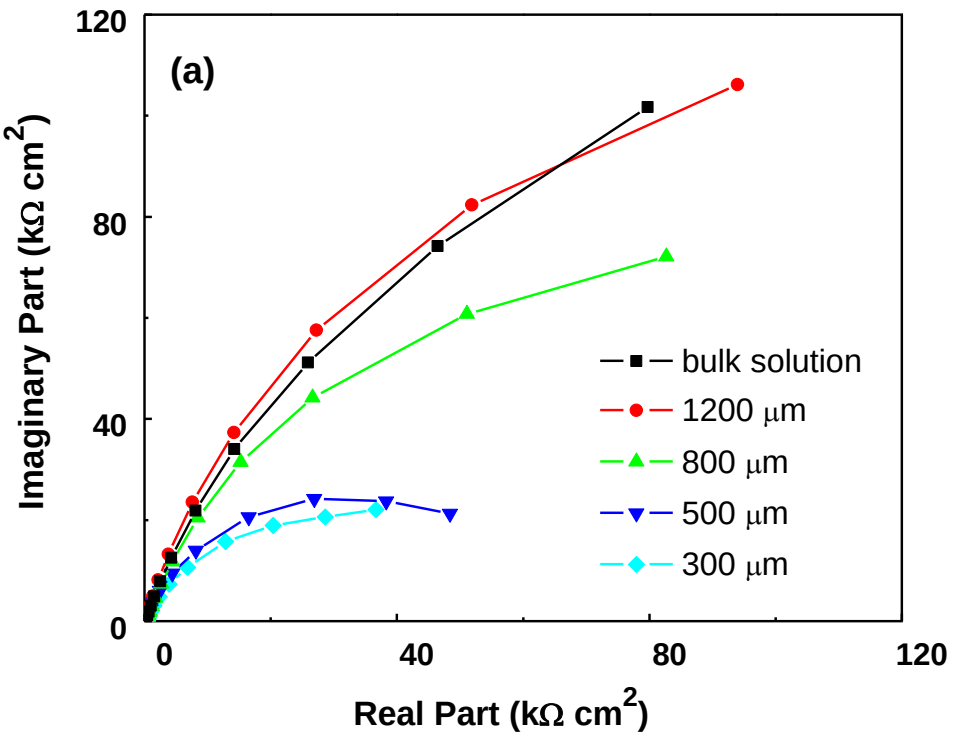

(b)

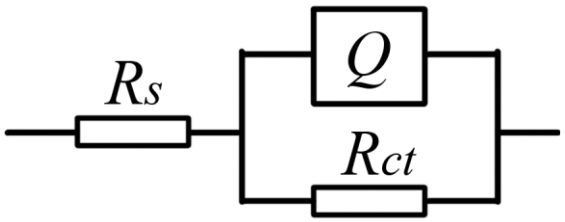

Figure 4. Nyquist (a) diagram and Randle equivalent circuit (b) for 304 SS in 0.5 wt. % NaCl under different layers.

Nyquist spectras all show one apparent capacitive semicircle and most of the phase shift exceed -45^{o} when presented on a Bode diagram. This suggests that the current distribution on the surface of the electrode is even in EIS tests. According to the corrosion process of SS under neutral sodium chloride solution and the morphologies of the corroding surface, and with the similar results and referring to Nishikata' work and TML model [15], the *R(QR)* Randle equivalent circuit was adopted to fit the EIS plots (Fig.4b), where R_s is the solution resistance, R_{ct} is the charge transfer resistance resulting from the formation of ionically conducting paths across the passive layer, Q denotes the double layer capacitance. The fitted parameters are listed in Table 3.

Table 3. The fitted EIS parameters for 304 SS in 0.5 wt. % NaCl under different layers.

Layer thickness (μm)	R_s (Ω cm^2)	Q (μF cm^{-2})	n	R_{ct} (Ω cm^2)
Bulk solution	99.6	6.44×10^{-5}	0.83	3.22×10^{5}
1200	123.7	6.14×10^{-5}	0.86	2.95×10^{5}
800	191.7	6.67×10^{-5}	0.80	2.22×10^{5}
500	278.1	8.16×10^{-5}	0.82	6.71×10^{4}
300	360.2	1.05×10^{-4}	0.80	5.93×10^{4}

Results tabulated in Table 3 demonstrate that as the thickness of electrolyte layers decreases, the solution resistance (R_s) increases and R_{ct} decreases.

In this study, the reciprocal of R_{ct} was taken as a parameter to characterise the corrosion rate and the values of charge transfer resistance (R_{ct}) for different electrolyte layers were calculated from the medium frequency range. The relationship between the thicknesses of the electrolyte layers and i_{corr}, $1/R_{ct}$ is shown in Fig.5.

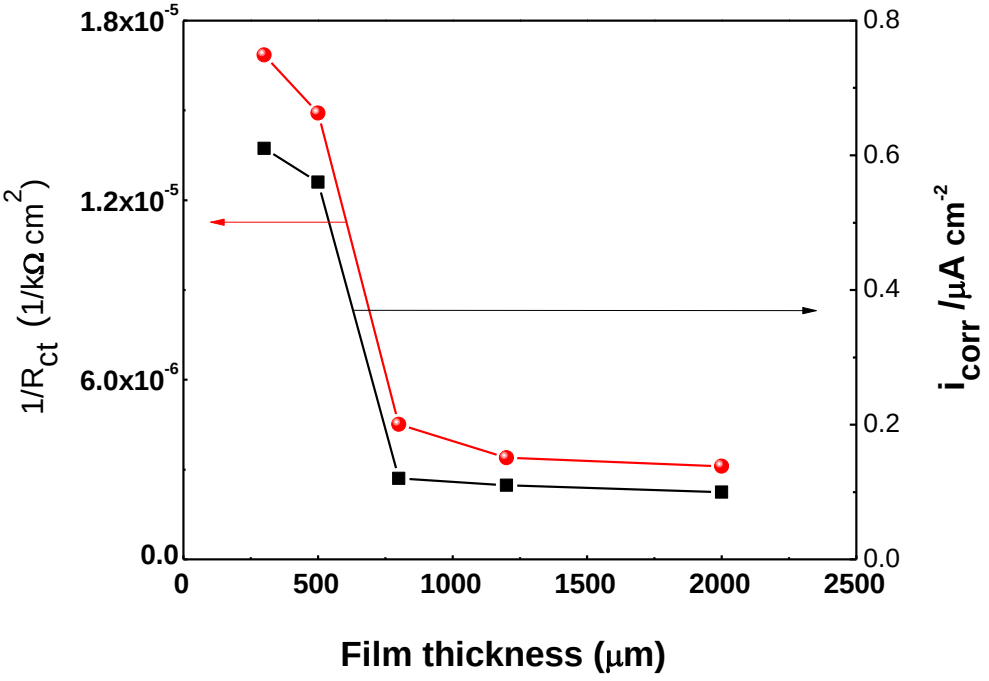

Figure 5. Relationship between the thicknesses of the electrolyte layers and the I_{corr}, $1/R_{ct}$.

The two plots are very similar to each other demonstrating that when the thicknesses of the thin electrolyte layers decrease, the corrosion progress of 304 SS was noticeably accelerated. Moreover, it is worth noticing that when the thicknesses of the electrolyte layers were less than 800 μm, both plots changed sharply. Conversely it was noticed that when the thickness of the electrolyte layers was greater 800 μm, there was little variation in the corrosion rates. It is known that the corrosion rate is determined by the cathodic and anodic processes; therefore the change of the corrosion rates in this study can be analysed based on the influence of the thickness of the electrolyte layers.

From these results, it was found that the corrosion behaviour of 304 SS under thin electrolyte layers was distinctively different from that of carbon steel, often producing a visible corrosion and corrosion products. With the hydration of dissolved metal ions becoming more difficult, the anodic process can be inhibited significantly and the anodic current density was lower than that in bulk solution [14]. This is because the surface of 304 SS is covered by a very thin but compact passive film, which can form spontaneously.

3.2 Effects of chloride concentration on the corrosion behaviour of 304 SS

Fig.6 shows the polarization curves measured for 304 SS in 0.1 wt. %, 0.5 wt. % and 3.5 wt. % NaCl under different layers: (a) 300 μm; (b) 500 μm.

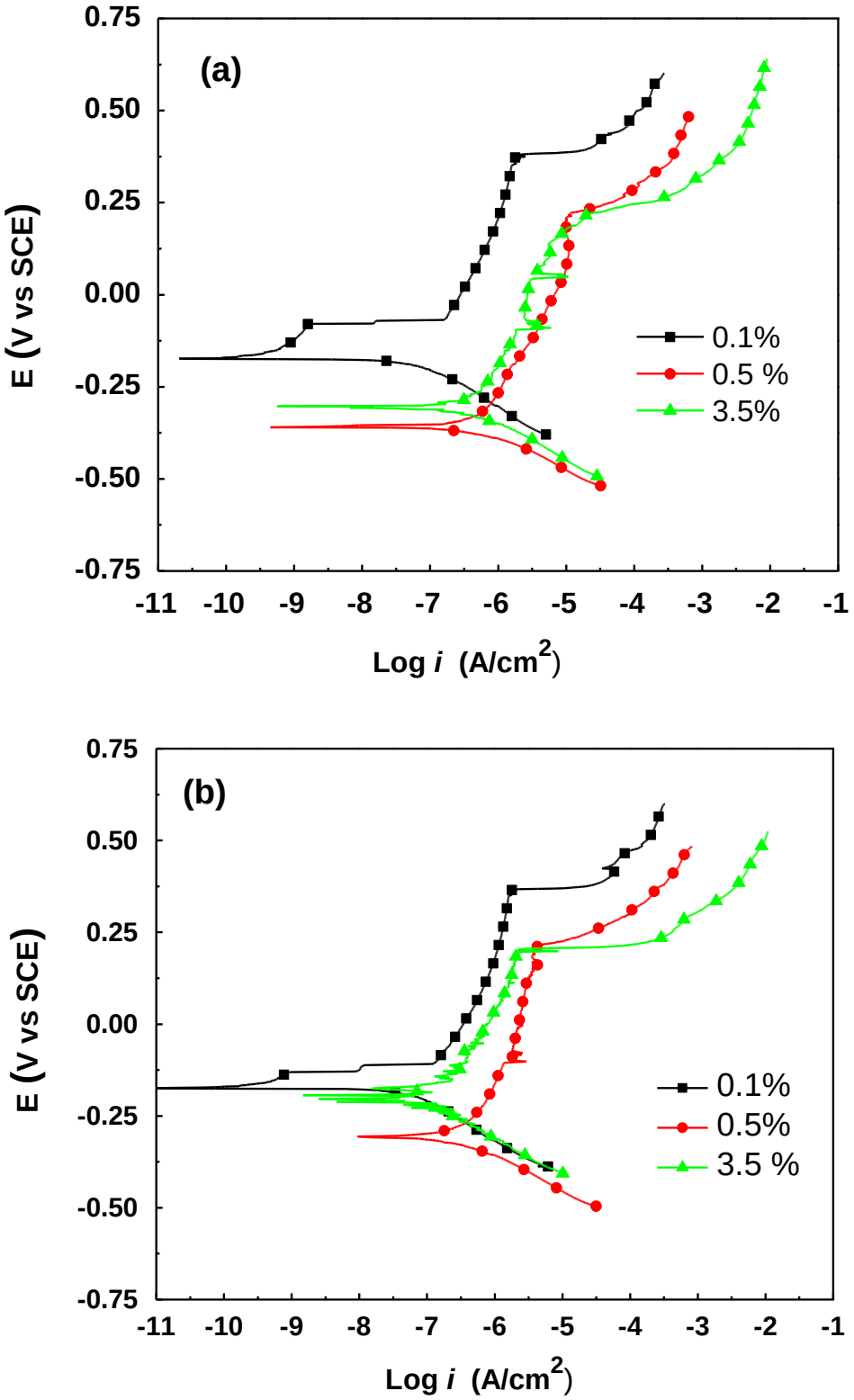

Figure 6. Polarization curves measured for 304 SS in 0.1 wt. %, 0.5 wt. % and 3.5 wt. % NaCl under different layers: (a) 300 μm; (b) 500 μm.

When the thickness of the electrolyte layer was at 300 μm and 500 μm, the trend of the polarization curves had no difference. When the chloride concentration increased from 0.1 wt. % to 0.5

wt. %, E_{corr} and E_p became more negative and i_{corr} and i_p increasing. This indicated that the increase of Cl^- ions would accelerate the atmospheric corrosion and decrease the pitting resistance of 304 SS. However, when the chloride concentration reaches up to 3.5 wt. %, i_{corr} and i_p were slightly improved.

The relationship between the chloride concentration and E_p is shown in the Fig.7.

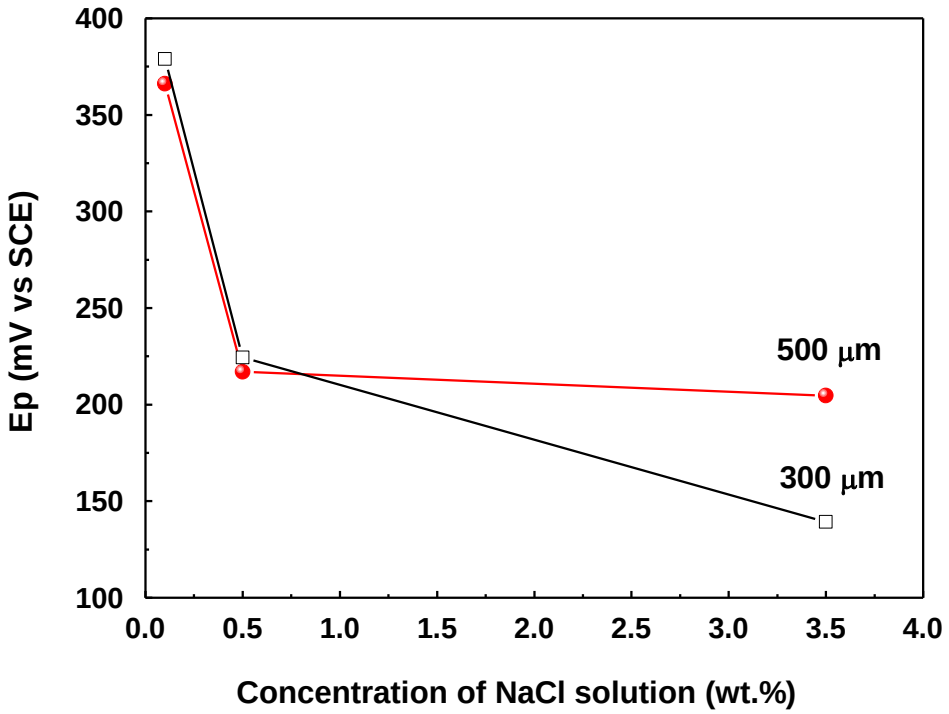

Figure 7. Pitting potential for 304 SS in 0.1 wt. %, 0.5 wt. % and 3.5 wt. % NaCl under different layers.

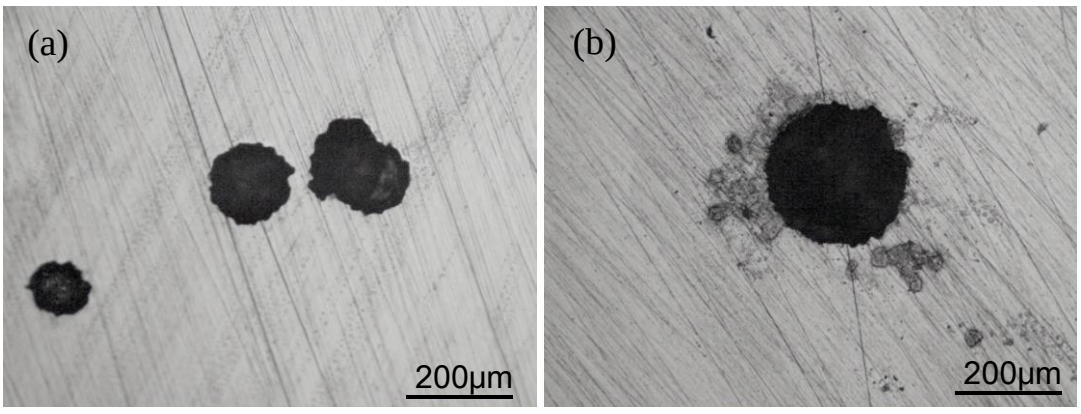

Figure 8. Pit morphologies of 304 SS in 3.5 wt. % NaCl after polarization under different layers: (a) 300 μm; (b) 500 μm.

When the Cl^- ions concentration increases from 0.1 wt. % to 0.5 wt. %, the E_p decreased dramatically. However when the concentration of the chloride solution was increased from 0.5 wt. % to 3.5 wt. %, E_p shows two different trends: one was that when the thickness of electrolyte layer was at

300 μm, a clear decrease in E_p can be seen. It was also noticed that as the Cl^- ions concentration increased at an electrolyte layer thickness of 500 μm, the drop of E_p was negligible. Fig.8 shows the pit morphologies of 304 SS in 3.5 wt. % NaCl after polarization under different layers: (a) 300 μm; (b) 500 μm.

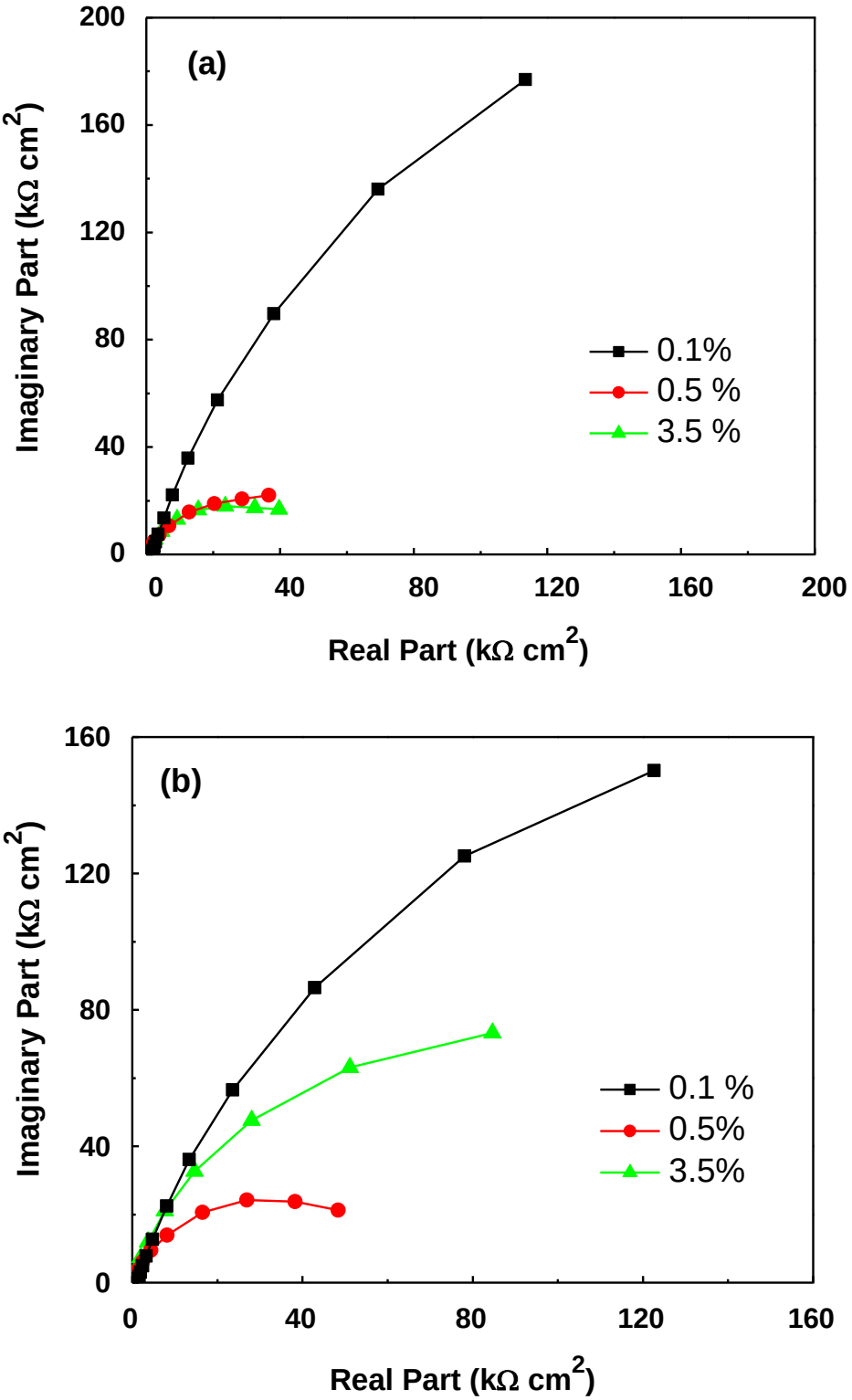

Figure 9. Nyquist diagrams for 304 SS in 0.1 wt. %, 0.5 wt. % and 3.5 wt. % NaCl under different layers: (a) 300 μm; (b) 500 μm.

Optical microscope analysis revealed that with a thinner electrolyte layer, an increased amount of smaller pits had formed on the surface of the SS samples. The growth of pits may be restrained by the quick saturation of metal ions. Although the saturation of metal ions could easily happen within a limited amount of solution and a higher concentration of Cl^- ions, the dissolution rate in the centre of the pit maybe reduced, however the pits are still bigger than that in dilute electrolyte layers (seen in Fig.3) [15, 26, 27].

Fig.9 shows the Nyquist diagrams for 304 SS in 0.1 wt. %, 0.5 wt. % and 3.5 wt. % NaCl under different layers: (a) 300 μm; (b) 500 μm.

EIS results show one apparent capacitive semicircle for all tests carried out. Parameters listed in Table 4 show that as the concentration of Cl^- ions increased, R_{ct} reduced initially and then increased, which is well within the polarization measurements.

Table 4. The fitted EIS parameters for 304 SS in 0.1 wt. %, 0.5 wt. % and 3.5 wt. % NaCl under 500 μm and 300 μm layers.

Concentration NaCl (wt.%)	Layer thickness (μm)	R_s (Ω cm^2)	Q (μF cm^{-2})	n	R_{ct} (Ω cm^2)
0.1	500	917	3.89×10^{-5}	0.82	5.20×10^{5}
	300	1271	3.92×10^{-5}	0.81	9.00×10^{5}
0.5	500	278.1	8.16×10^{-5}	0.82	6.71×10^{5}
	300	360.2	1.05×10^{-5}	0.80	5.90×10^{5}
3.5	500	43.65	6.77×10^{-5}	0.86	1.84×10^{5}
	300	73	8.50×10^{-5}	0.83	4.99×10^{4}

Compared with the electrochemical behaviour of 304 SS in bulk solution, E_{corr} showed a significant shift in the negative direction under thin electrolyte layers. The variations of i_p were not the same as that of E_p, while both of them linearly decreased in bulk solution. It can be explained that as the Cl^- ions concentration increased from 0.5 wt. % to 3.5 wt. %, dissolved oxygen in thin electrolyte

layers might reduce, which could be attributed to the salt effect of oxygen [11, 12, 14]. With a limited amount of solution, a saturation of chloride solution could quickly form around the corroded area, resulting in the dissolution of metals becoming slightly inhibited. As a result, i_p in 3.5 wt. % NaCl reduced less than that in 0.5 wt. % NaCl. At very thin electrolyte layers (less than 300 μm) this is because of a faster transmission of oxygen. However a higher Cl^- ions concentration could strongly induce the dissolution of metals, with E_p representing a linearly decreasing trend. The EIS results and pit morphologies also agreed with the above analysis.

4. CONCLUSIONS

The corrosion of 304 SS under various thicknesses of thin electrolyte layers containing chloride ions has been studied by the potentiodynamic polarization and the EIS method. The potentiodynamic polarization measurements showed that, as the thickness of the electrolyte layers decreased, pitting potentials reduced, and maintaining passivity current densities increased, especially under the layers less than 800 μm. This is probably caused by an easier transmission of oxygen, which not only promoted the formation of a passive film at the initial corrosion process with a higher i_{corr}, but also decreased the thickness of the chromium-rich passive film resulting in an increased dissolution rate with a lower E_p and a higher i_p.

The EIS measurements showed that the corrosion rate under thin electrolyte layers increased as the concentration of Cl^- ions increased from 0.5 wt. % to 3.5 wt. % with the dissolution of metals being slightly inhibited. This corresponded well with the results collected from polarization measurements and pit morphologies. It is thought that this is due to a reduced amount of dissolved oxygen within the thin electrolyte layer, resulting in the ability of mass transport being reduced, This was especially true for the corrode areas, where metal ions easily saturated when a pit initiated. Besides, although individual pits were inhibited and became smaller, an increased amount of pits were observed under the thin electrolyte layers reflecting a higher corrosion rate. But as the strong pitting inducement of a high Cl^- ions concentration, E_p decreased linearly.

ACKNOWLEDGEMENTS

The authors acknowledge the support of National Natural Science Foundation of China (No. 51671028), the National Key Research and Development Program of China (No. 2016YFB0300604, 2016YFB0700502) and the National Basic Research Program of China (973 Program project, No. 2014CB643300).

References

1. M. Kimura, K. Suzuki, M. Kusaka, K. Kaizu, *J. Mater. Process.*, 26 (2017) 178.
2. X. Cheng, Z. Jin, M. Liu and X. Li, *Corros. Sci.*, 115 (2017) 135.
3. H. S. Klapper, J. Goellner, A. Burkert, *Corros. Sci.*, 75 (2013) 239.
4. K.H. Lo, C.H. Shek, J.K.L. Lai, *Mater. Sci. Eng. R*, 65 (2009) 39.
5. X.G. Li, D.W. Zhang, Z.Y. Liu, Z. Li, C.W. Du and C.F. Dong, *Nature*, 527 (2015) 441.

6. G.T. Burstein, S.P. Vines, *J. Electrochem. Soc.*, 148 (2001) B504.
7. X.Q. Cheng, Y.W. Tian, X.G. Li and C. Zhou, *Mater. Corros.*, 65 (2014) 1033.
8. W. Tian, N. Du, S. Li, S. Chen and Q. Wu, *Corros. Sci.*, 85 (2014) 372.
9. H. Huang, Z. Pan, X. Guo and Y. Qiu, *Corros. Sci.*, 75 (2013) 100.
10. N.D. Tomashov, *Corrosion*, 20 (1964) 7.
11. Y. Tsutsumi, A. Nishikata, T. Tsuru, *Corros. Sci.*, 49 (2007) 1394.
12. M. Stratmann, H.Streckel, *Corros. Sci.*, 30 (1990) 681.
13. M. Stratmann, H. Streckel, *Corros. Sci.*, 30 (1990) 697.
14. M. Stratmann, H. Streckel, *Corros. Sci.*, 30 (1990) 715.
15. A. Nishikata, Y. Ichihara, T. Tsuru, *Corros. Sci.*, 37(1995) 897.
16. A. Nishikata, F. Suzuki, T. Tsuru, *Corros. Sci.*, 47 (2005) 2578.
17. Y.L. Cheng, Z. Zhang, F.H., *Corros. Sci.*, 46 (2004) 1649.
18. U.R. Evans, *Nature*, 206 (1965) 980.
19. U.R.Evens, *Edward Arnold Ltd., London*, 1982: 13-24.
20. F. Mansfeld, S.Tsai, *Corros. Sci.*, 20 (1980) 853.
21. F. Mansfeld, M.W. Kandig, S. Tsai, *Corros. Sci.*, 22 (1982) 455.
22. M. Legrand, B. Diawara, J. J. Legendre and P. Marcus, *Corros. Sci.*, 44 (2002) 773.
23. Y. Wang, X. Cheng, X. Li, *Electrochem. Commun.*, 57 (2015) 56.
24. S. Krakowiak, K. Darowicki, P. Slepski, *Electrochim. Acta.*, 50 (2005) 2699.
25. M. Dornhege, Punckt, J.L. Hudson and H.H. Rotermund, *J. Electrochem. Soc.*, 154 (2007) 24.
26. T. Li, L. Liu, B. Zhang, Y. Li and F. Wang, *Corros. Sci.*, 111 (2016) 186.
27. P. Ernst, R.C. Newman, *Corros. Sci.*, 44 (2002) 943.